SLAC – PUB – 4339 (REV)
March 1988
(A/E)

DISRUPTION EFFECTS FROM THE INTERACTION OF ROUND e^+e^- BEAMS*

PISIN CHEN

Stanford Linear Accelerator Center,
Stanford University, Stanford, California 94309

KAORU YOKOYA

KEK, National Laboratory for High Energy Physics,
Ohi–Machi,Tsukuba, Ibaraki 305, Japan

ABSTRACT

We report on our recent simulation results on the disruption effects during the interaction of round e^+e^- beams in linear colliders. It is found that in addition to the well-known disruption parameter, D, the disruption effects also depend on another parameter $A \equiv \sigma_z/\beta^*$, where σ_z is the bunch length and β^* the β–function at the interaction point. It turns out that while the luminosity enhancement factor, H_D, is insensitive to A only in the small $D(D \lesssim 1)$ regime, the disruption angle enhancement factor, H_θ, behaves oppositely. Specifically, we found that for large D, H_θ is suppressed as $1/\sqrt{D}$, and H_D increases monotonically without saturation. Moreover, for fixed D, H_D varies as a function of $\ell n(1/A)$. Computer analysis further suggests that in the large D and small A regime a confinement mechanism is developed near the beginning of the collision: particles once pinched tend to be trapped in a much smaller radius throughout the process. A theoretical model is provided to qualitatively explain the above findings.

Submitted to *Physical Review D*

*Work supported by the Department of Energy, contract DE–AC03–76SF00515.

1. INTRODUCTION

To achieve high enough luminosity for particle physics experiments in linear colliders, it is necessary to focus the colliding e^+e^- beams down to miniscule dimensions at the interaction point. In the world's first of such accelerators, the Stanford Linear Collider (SLC), the beam size at the interaction point is designed to be $\sigma_0 \equiv \sigma_x = \sigma_y = 1.65\ \mu$m, and $\sigma_z = 1$ mm.[1] For the next generation of linear colliders at the range of 1 TeV in the center-of-mass energy, the beam size would be even smaller. The high density of charged relativistic particles would provide strong electromagnetic fields viewed by the particles of the oncoming beam, while the particles in the same bunch feel no space-charge effects to the order of $1/\gamma^2$. Two major effects arise during this beam-beam interaction which are important to the design of linear colliders. Namely, the *disruption* effect associated with the bending of particle trajectories under the influence of these EM fields provided by the oncoming beam; and the *beamstrahlung* effect associated with radiation loss of the particle energies induced by the bending of the trajectories.

Strictly speaking, the two effects, disruption and beamstrahlung, are coupled. This is self-evident because without deflection there would be no radiation, and with radiation during bending the remaining trajectory of the particle would not be the same. Fortunately, in a large range of beam parameters the average disruption angle is rather small, and the emission of hard photons is relatively rare. For these reasons the two effects can be isolated from each other to the first degree and the studies of the issues are greatly simplified.

In this paper we present new computer simulation results on disruption effects assuming negligible beamstrahlung. The same subject has been previously investigated by several authors. While the well-known results of Hollebeek[2] on

the functional behavior of the luminosity enhancement factor has long been accepted, the recent study of Fawley and Lee[3] hints on discrepancy in the large disruption regime. Considering the importance of luminosity for high energy experiments, it seems profitable to reinvestigate the issue with more detailed simulations. In particular, our attention has been directed to the exceedingly high local particle densities due to beam focusing, which can contribute significantly to the luminosity and might affect the eventual disruption angles, as well.

The paper is roughly constructed in two parts. In the first part, we present the simulation results on the average and the maximum disruption angles in Section 2 and the luminosity enhancement factor in Section 3. In both sections simple semi-empirical scaling laws are given to fit the simulation results. The second part of the paper is devoted to a theoretical model which qualitatively explains the simulation results on the luminosity enhancement factor. To do this, we investigate the time evolution of the differential luminosity near the end of Section 3. It is found that the disruption processes are characteristically different in three regimes of the disruption parameter D, defined as

$$D = \frac{r_e \sigma_z N}{\gamma \sigma_0^2} \quad , \tag{1.1}$$

where r_e is the classical electron radius and γ the Lorentz factor of the relativistic beam. Sections 4, 5 and 6 deal with theoretical descriptions for the small ($D \lesssim 0.5$), medium ($0.5 \lesssim D \lesssim 5$) and large ($D > 5$) disruption regimes, respectively. The small D regime corresponds to the situation where the first focal point of one beam lies beyond the oncoming beam. As such, the oncoming beam can be regarded as a weak focusing lens. In the medium D regime, the focal point starts to lie inside the oncoming beam, and a large fraction of the beam disrupts

severely after being focused. The situation changes dramatically as the interaction passes into the large D regime. It is found that the beam during pinching evolves into a *core* and a *halo* in its transverse distribution where the core, once formed, tends to be confined in an equilibrium radius throughout the remainder of the collision.

In all these studies of the disruption effects we introduce, in addition to D, another Lorentz invariant, dimensionless parameter A, defined as

$$A = \frac{\sigma_z}{\beta^*} \quad , \tag{1.2}$$

where β^* is the β–function at the interaction point of the e^+e^- beams.

Physically, A measures the inherent divergence of the incoming beam. This is important because the collision process takes place within several σ_z's around the interaction point, and the natural variation of the beam size over such a distance due to the finiteness of the β–function would have a significant impact on the disruption process. In the study of disruption effects one often chooses to fix the beam size σ_0 at the interaction point so that the nominal luminosity (in the absence of disruption) can be computed. In such a case, A is related to the invariant emittance ϵ_n via the relation $A = \epsilon_n \sigma_z / \gamma \sigma_0^2$. Furthermore, one can easily verify that A/D manifests the initial phase space area per particle of the beam in units of the classical electron radius:

$$\frac{A}{D} = \frac{\epsilon_n}{r_e N} \quad , \tag{1.3}$$

which is independent of the optics that the beam experiences.

In this paper we assume the same initial parameters for the colliding electron and positron beams. The longitudinal coordinate s is fixed to the center-of-mass frame whose origin is the collision point of the two bunch centers. The time coordinate t is defined such that $t = 0$ when the two bunch centers collide. We further introduce the longitudinal coordinates z_j $(j = 1, 2)$ co-moving with the two bunches. The origin of z_j is the center of the jth bunch, and z_j is positive along the direction of motion of the beam (see Fig. 1). In our calculations we shall ignore the longitudinal component of the focusing force, which is of the order $1/\gamma$ smaller than the transverse component. Thus, the coordinate z_j of a particle is a constant in t. It is easy to see that particles in one bunch that arrive at s at time t should have their co-moving coordinate z_1 related to s by

$$s = z_1 + t \quad , \tag{1.4}$$

where we adopt the convention that the speed of light $c = 1$. On the other hand, particles in the opposite bunch arriving at the same space-time point would have their co-moving coordinate z_2 related by

$$s = -z_2 - t \quad . \tag{1.5}$$

With these relations in mind, the luminosity for $A = 0$ is defined by

$$\mathcal{L}_0 = 2fN^2 \int dxdydsdt \; n_1(x, y, z_1, t) \; n_2(x, y, z_2, t) \quad , \tag{1.6}$$

where f is the repetition rate of collisions, and $n_j(x, y, z_j, t)$ the distribution function of the jth beam at time t, normalized such that

$$\int n_j(x, y, z_j, t) \; dxdydz_j = 1 \quad , \quad j = 1, 2 \quad . \tag{1.7}$$

Since we ignore the longitudinal force, the longitudinal distributions are constant in time, i.e.,

$$\int n_j(x,y,z_j,t)\,dxdy \;=\; n_z(z_j) \;=\; \frac{1}{\sqrt{2\pi}\sigma_z}\,\exp\left\{-\frac{z_j^2}{2\sigma_z^2}\right\} \quad . \tag{1.8}$$

In the absence of disruption, the luminosity in Eq. (1.6) can be straightforwardly integrated (assuming Gaussian distributions) to get

$$\mathcal{L}_0 \;=\; \frac{fN^2}{4\pi\sigma_0^2} \quad . \tag{1.9}$$

When $A \neq 0$, the above expression should be modified to take into account the variation of the beam cross section due to the change of the β–function around the interaction point. This can be done by introducing a reduction factor η_A:

$$\eta_A = \frac{2}{\sqrt{\pi}\sigma_z}\int_0^\infty \frac{e^{-z^2/\sigma_z^2}}{1+z^2/\beta^{*2}}\,dz \quad , \tag{1.10}$$

such that the luminosity for a finite A in the absence of disruption is[4]

$$\mathcal{L}_A = \eta_A \mathcal{L}_0 \quad . \tag{1.11}$$

Numerically, $\eta_A \simeq 0.76$ at $A = 1.0$, and rapidly approaches unity for $A < 1$. Since a reasonably designed accelerator would presumably be chosen to work in the regime where $A < 1$ to avoid degradation on luminosity, we find it convenient to use $\mathcal{L}_0$ as a reference parameter for all values of A.

When the disruption is included, the effective luminosity $\mathcal{L}$ would be different from $\mathcal{L}_0$, and a luminosity enhancement factor H_D is introduced to account for the change

$$H_D \equiv \frac{\mathcal{L}}{\mathcal{L}_0} \quad . \tag{1.12}$$

Note that with H_D so defined, and without η_A involved, it is possible that $H_D \lesssim 1$ when D is small but A is large.

By the same token, we introduce a disruption angle enhancement factor H_θ. In the weak focusing limit where $D \ll 1$, the approximate solution of the equation of motion for a particle with impact parameter r_0 can be shown to be

$$\left.\frac{dr}{dt}\right|_{final} \sim -\frac{r_e N}{\gamma \sigma_0^2} r_0 \quad . \tag{1.13}$$

Thus, the nominal disruption angle can be defined as

$$\theta_0 = \frac{r_e N}{\gamma \sigma_0} \quad . \tag{1.14}$$

The effective disruption angles θ_D for an arbitrary D is generally different from θ_0, so H_θ is defined as

$$H_\theta \equiv \frac{\theta_D}{\theta_0} \quad . \tag{1.15}$$

The computer code, developed by one of us (KY) earlier,[5] is now named ABEL (Analysis of Beam–beam Effects in Linear colliders). In the code the initial conditions of the macroparticles, typically 40,000 to 60,000 in number for each beam, are created at once at $s = 0$ by Gaussian random numbers in five dimensions, σ_x, σ_x', σ_y, σ_y' and σ_z. These macroparticles are then traced

back to their locations where the simulation starts. Each beam is sliced into longitudinal meshes with thickness typically $\sim 0.05\,\sigma_z$. In each mesh the particles are subdivided into transverse bins where the two-dimensional Poisson equation is solved to find the local electrostatic force that act on the opposite bunch. The magnetic force is assumed to be equal in magnitude to the electrostatic force. The particles are then pushed according to the equation of motion solved by the central difference method.

In the original version of ABEL, the Poisson equation was solved by using a band matrix as described in Ref. 5. Since then, two major improvements have been introduced for faster and more accurate computations. One of these utilizes Fast Fourier Transformation (FFT) in two dimensions. This enables one to handle the transverse bin size down to as small as $0.1\,\sigma_0$. This method would still take a considerable amount of computing time if an even smaller bin size is required, as is the case in the large D regime. The other method, which is used for the simulations presented in this paper, assumes axial symmetry of the particle distribution at every time step and integrates the Poisson equation simply by

$$\text{radial field} \sim \frac{1}{r}\int_0^r n(r)\,r\,dr \quad . \tag{1.16}$$

In practice, since the initial conditions of the finite number of macroparticles are generated by random numbers, there are tiny fluctuations around the assigned particle distribution that break the axial symmetry. Nevertheless, Eq. (1.16) is still invoked to calculate the pinch force, while the fluctuations in the distribution are traced. Compared to the first method (FFT), this method is much faster, and thus allows for much smaller radial bin size, which is necessary for our purpose to monitor very high local densities during the collision.

The radial bin size used in our simulations is anywhere between 1/20 and 1/200 of σ_0, depending on the values of D and A. Larger D and smaller A require smaller bin sizes. It should be mentioned that in simulations the actual beam size is truncated at $\pm 2.5\ \sigma$ in both longitudinal and transverse directions. Accordingly, the luminosity $\mathcal{L}_0$ differs from Eq. (1.9) by a few percent. This slight correction has been taken into account in all our calculations. With the beam size so chosen, the beams move through each other in 800 to 1600 time steps. A typical computing time for one run is between 30 seconds and 3 minutes.

Constrained by the axial symmetry that we imposed, our present study is thus limited to cases for exactly head-on collisions (but random fluctuations are allowed) of round beams (i.e., $\sigma_x = \sigma_y = \sigma_0$) only. Nonaxisymmetric problems such as flat beam (i.e., $\sigma_x > \sigma_y$) collisions, effects due to beam alignment offset, collision with a crossing angle, etc., still await future efforts.

2. DISRUPTION ANGLES

One important piece of information for linear collider design is the expected disruption angle. Knowledge of the maximum disruption angle is essential to determine the aperture of the last element in a final focusing system, so as to avoid being showered by the debris from the beam-beam collision.

The simulation results of the maximum and the *rms* disruption angle enhancement factors, H_θ^{max} and H_θ^{rms}, are plotted in Figs. 2 and 3, respectively. The curves for $A = 0$ in the two figures reasonably agree with the previous results.[6] These curves for zero emittance can be well-explained theoretically,[7] which predicts the following generic functional behavior for both $H_{\theta,0}^{max}$ and $H_{\theta,0}^{rms}$ for $A = 0$, i.e., a linear increase for $D \ll 1$ and a $1/\sqrt{D}$ suppression for $D \gg 1$:

$$H_{\theta,0} \sim \begin{cases} a + bD\,, & D \ll 1\,, \\ \dfrac{c}{\sqrt{D}}\,, & D \gg 1\,, \end{cases} \tag{2.1}$$

where a, b and c are some numerical coefficients which are different for maximum and *rms* angles, and which are to be fixed by the simulations. From Figs. 2 and 3 we find

$$H_{\theta,0}^{max} \simeq \begin{cases} 0.87 + 1.57\ D\,, & D \ll 1\,, \\ \dfrac{1.84}{\sqrt{D}}\,, & D \gg 1\,, \end{cases} \tag{2.2}$$

and

$$H_{\theta,0}^{rms} \simeq \begin{cases} 0.78 + 0.20\ D\,, & D \ll 1\,, \\ \dfrac{0.67}{\sqrt{D}}\,, & D \gg 1\,. \end{cases} \tag{2.3}$$

When $A \neq 0$, the inherent divergence of the beam cannot be overlooked when the disruption is small. The natural *rms* divergence angle of a beam is

$$\sigma'_{x,y} = \frac{\sigma_{x,y}}{\beta^*} = \frac{\sigma_0}{\beta^*}\,, \tag{2.4}$$

while

$$\sigma_0' \;=\; \sqrt{\sigma_x'^2 + \sigma_y'^2} \;=\; \sqrt{2}\,\sigma_x' \;. \tag{2.5}$$

Dividing both sides by θ_0, as defined in Eq. (1.12), we have the contribution from finite emittance:

$$H_{\theta,\epsilon}^{rms} \;\equiv\; \frac{\sigma_0'}{\theta_0} \;= \sqrt{2}\,\frac{A}{D}\;, \tag{2.6}$$

where the definitions of A and D are used. The general expression for H_θ^{rms} is therefore

$$H_\theta^{rms} \;=\; \sqrt{(H_{\theta,0}^{rms})^2 + (H_{\theta,\epsilon}^{rms})^2} \quad . \tag{2.7}$$

Inserting Eq. (2.3) for $H_{\theta,0}^{rms}$ and Eq. (2.6) for $H_{\theta,\epsilon}^{rms}$, the above expression fits all the curves in Fig. 3 very well. Notice that the contribution of the second term rapidly diminishes for D beyond unity. Thus, the *rms* disruption angle is asymptotically independent of A.

The situation for the maximum disruption angle is slightly more complicated, since the maximum natural divergence angle for Gaussian distributions is not well-defined. However, as is the case for $H_{\theta,0}$, the functional behavior of $H_{\theta,\epsilon}^{max}$ should be similar to that of $H_{\theta,\epsilon}^{rms}$, and the overall H_θ^{max} should be analogous to H_θ^{rms}, in Eq. (2.7). This is evidenced by the similarity between Figs. 2 and 3, aside from the numerical differences.

3. LUMINOSITY ENHANCEMENT FACTOR

From the disruption process, our major concern is the effective luminosity $\mathcal{L}$ compared to the nominal luminosity $\mathcal{L}_0$, or the luminosity enhancement factor H_D. As is mentioned in the Introduction, H_D is a function of both D and A. In the design of a linear collider, it is desirable to have A considerably smaller than unity, otherwise the luminosity would be degraded because of the significant variation of the beam size during collision due to the finiteness of β^*.

Figure 4 shows H_D as a function of D for five values of A ($A = 0.05$, 0.1, 0.2, 0.4 and 0.8). Notice that for relatively small values of D, say $D \lesssim 5$, the result of Hollebeek's,[2] which was evaluated at $A = 0$, seems to agree roughly with our curve for $A = 0.2$. In fact, in this region of D our result also agrees with that of Fawley and Lee,[3] which was evaluated at $A = 0.2$. However, there is a novel feature which was not observed before, namely, H_D varies for different values of A. In our simulations the five values of A are selected such that they are equally spaced in logarithmic scale. One finds from the figure that for each D the curves for different A's are roughly equally separated except for large A (e.g., $A \gtrsim 0.8$), where the separation depends on D. This suggests that H_D has a term proportional to $\ell n(1/A)$ for small A, i.e.,

$$\lim_{A\to 0} H_D \propto \ell n\left(\frac{1}{A}\right) \quad , \qquad \text{for fixed } D \quad . \tag{3.1}$$

Another characteristic feature of our result is the monotonic increase of H_D as a function of D (for all A's) at least up to $D = 100$. This is fundamentally different from Hollebeek's result where the luminosity enhancement saturates at the value $H_D \sim 6$ beyond $D \sim 5$ and decreases for $D \gtrsim 20$. On the other hand,

our result agrees with that of Fawley and Lee in this respect, except that the rate of increase in H_D in Fig. 4 turns out to be more pronounced than that of Fawley–Lee. Here again, H_D unmistakably depends on A in the large D regime.

These differences between the simulations, we think, are brought about mainly by the resolution in the transverse dimensions. As long as A is small, the particle density during collision is rather singular near the axis. As would be discussed in much more detail in Section 6, in the large D regime the beam tends to develop itself into a *core* and a *halo*. While the size of the halo, which can be estimated by naïve geometric considerations, is of the order

$$\sigma_{halo} \sim \frac{\sigma_0}{\sqrt{H_D}} \quad , \tag{3.2}$$

the size of the core is roughly

$$\sigma_{core} \sim \frac{A}{\sqrt{D}} \sigma_0 \quad . \tag{3.3}$$

Thus the core is much smaller in size, and it requires good resolution in simulations in order not to overlook the contribution from the core.

Based on the data shown in Fig. 4, an expression for H_D is found on purely empirical grounds:

$$H_D = 1 + D^{1/4} \left(\frac{D^3}{1+D^3} \right) \left[\ell n(\sqrt{D}+1) + 2\, \ell n \left(\frac{0.8}{A} \right) \right] \quad . \tag{3.4}$$

This expression reproduces all the data in Fig. 4 to an accuracy of around $\pm 10\%$. Equation (3.4), however, differs substantially from the corresponding expression given in Ref. 7, where the fit was based upon the middle three curves in Fig. 4 then available.

In order to analyze the physical mechanism of the disruption process which give rise to the H_D behavior shown in Fig. 4, we investigate the time evolution of H_D. The differential luminosity (per unit time), $d\mathcal{L}/dt$, can be defined as

$$\frac{d\mathcal{L}}{dt} = 2f N^2 \int dxdyds\, n_1(x,y,z_1,t)\, n_2(x,y,z_2,t) \quad . \tag{3.5}$$

By the same token, the differential luminosity enhancement factor, dH_D/dt, is defined by

$$\frac{dH_D}{dt} = \frac{1}{\mathcal{L}_0} \frac{d\mathcal{L}}{dt} \quad , \tag{3.6}$$

such that

$$H_D = \int_{-\infty}^{\infty} \frac{dH_D}{dt}\, dt \quad . \tag{3.7}$$

In the absence of disruption, it is easy to see that

$$\frac{dH_D}{dt} = \frac{1}{\sqrt{\pi}\,\sigma_z} \exp\left\{\frac{-t^2}{\sigma_z^2}\right\} \quad , \tag{3.8}$$

and from this expression $\int (dH_D/dt)\, dt = 1$, by definition. Figure 5 shows dH_D/dt as a function of time for various values of D. Here, the parameter A is fixed at 0.05, and the time t is in units of σ_z/c. In spite of the fact that the H_D curves in Fig. 4 are reasonably smooth for each fixed value of A, the curves shown in Fig. 5 reveals different characteristics throughout the entire range of the value of D.

For very small D, e.g., $D \lesssim 0.5$, we find that dH_D/dt varies essentially as Eq. (3.8), which reflects the square of the longitudinal particle distribution of the bunch. When $D \sim 0.5$, a second peak appears at $t \simeq 1.6\ \sigma_z$/c. The peak

grows as D gets larger, and eventually becomes the dominant source for the luminosity enhancement by $D \simeq 0.7$. Notice also that the location of the second peak shifts gradually to the left as D increases, where the strong disruption induces the phenomena to occur earlier in time. Furthermore, while the buildup of the second peak becomes steeper, its falloff becomes smoother as D increases. This phenomena of a second peak appears in the region $0.5 \lesssim D \lesssim 5$. Beyond $D \sim 5$, the differential luminosity evolves into a new regime. The "second" peak now occurs right near the beginning of the collision, and its smooth *falloff* now recovers the Gaussian–like variation, except that there appear to be high-frequency wiggles superimposed. While the time evolution of dH_D/dt in both the small and the large D regimes behave similarly, their absolute values are distinctively different.

It turns out that the underlying physical mechanisms are indeed very different in the above mentioned three regimes of D, classified as follows: (1) the small D ($D \lesssim 0.5$), or the ***weak focusing*** regime, (2) the medium D ($0.5 \lesssim D \lesssim 5$), or the ***transition*** regime, and (3) the large D ($5 \lesssim D$), or the ***pinch confinement*** regime. In the following sections we shall provide theoretical descriptions that qualitatively explains the phenomena occurs in the three regimes.

4. THE WEAK FOCUSING REGIME

The weak focusing regime corresponds to the range $0 < D \lesssim 0.5$. For such small values of D, dH_D/dt is essentially described by the Gaussian function in Eq. (3.8). The correction to this expression to the first order in D can be derived in the following way. For the sake of argument we assume $A = 0$. This is justified because it turns out that there is no divergence at $A = 0$ in the correction term linear in D, i.e., to this order the correction arises only through the radial motions of the particles.

The equation of motion of a particle at z_1 in a bunch is

$$\frac{d^2r}{dt^2} = -\frac{4Nr_e}{\gamma} f_0(r)\, n_z(-2t - z_1) \ , \tag{4.1}$$

with

$$f_0(r) \equiv \frac{1}{r} \int_0^r n_{r0}(r)\, r dr \ , \tag{4.2}$$

where $n_{r0}(r)$ is the unperturbed radial distribution function normalized such that $\int n_{r0}(r)\ r dr = 1$. To derive the first order correction we had assumed unperturbed distribution on the right-hand side of Eq. (4.1). The solution of Eq. (4.1) with initial conditions $r = r_0$, and $dr/dt = 0$ at $t = -\infty$ is given by

$$r(t, z_1) = r_0 - \frac{4Nr_e}{\gamma} f_0(r_0)\ g(t, z_1) \quad , \tag{4.3}$$

with

$$g(t, z_1) = \int_{-\infty}^{t} dt_1 \int_{-\infty}^{t_1} dt_2\ n_z(-2t_z - z_1) = \int_{-\infty}^{t} dt_1\ (t - t_1)\ n_z(-2t_1 - z_1) \quad .$$

Equation (4.3) can be inverted as

$$r_0 \doteq r + \frac{4Nr_e}{\gamma} f_0(r)\, g(t, z_1) \quad , \tag{4.4}$$

within the same order of accuracy. For our purpose we like to know the perturbed radial distribution function $n_r(r)$ at (t, z_1). This can be found by

$$\begin{aligned} n_{r1}(r, t, z_1) &= n_{r0}(r_0)\, \frac{d(r_0^2)}{d(r^2)} \\ &= n_{r0}(r) \left[1 + \frac{4Nr_e}{\gamma} \left(\frac{1}{n_{r0}} \frac{dn_{r0}}{dr} f_0(r) + n_{r0}\right) g(t, z_1)\right] \quad . \end{aligned} \tag{4.5}$$

Accordingly, the luminosity can be evaluated as

$$\begin{aligned} \mathcal{L} &\propto \int r dr\, dz_1\, dz_2\, n_z(z_1)\, n_z(z_2) \Big[n_{r1}(r, t, z_1)\, n_{r1}(r, t, z_2)\Big]_{t=-(z_1+z_2)/2} \quad , \\ &= \int r dr\, dz_1\, dz_2\, n_z(z_1)\, n_z(z_2)\, [n_{r0}(r)]^2 \\ &\quad \times \left\{1 + \frac{4Nr_e}{\gamma} \left(\frac{1}{n_{r0}} \frac{dn_{r0}}{dr} f_0 + n_{r0}\right) \Big[g(t, z_1) + g(t, z_2)\Big]\right\}_{t=-(z_1+z_2)/2} \quad , \end{aligned} \tag{4.6}$$

where the leading term (unity) corresponds to the nominal luminosity $\mathcal{L}_0$. The integration over r can be carried out, which gives

$$\int_0^\infty r dr\, n_{r0}^2 \left(\frac{1}{n_{r0}} \frac{dn_{r0}}{dr} f_0 + n_{r0}\right) = \frac{1}{2} \int_0^\infty r dr\, n_{r0}^3 \quad . \tag{4.7}$$

Thus, the luminosity enhancement factor for small D is

$$\begin{aligned} H_D &\simeq 1 + \frac{4Nr_e}{\gamma} \left[\frac{\frac{1}{2} \int r dr\, n_{r0}^3}{\int r dr\, n_{r0}^2}\right] \\ &\quad \times \int dz_1\, dz_2\, n_z(z_1)\, n_z(z_2) \Big[g(t, z_1) + g(t, z_2)\Big]_{t=-(z_1+z_2)/2} \quad . \end{aligned} \tag{4.8}$$

Since the two colliding bunches are symmetric, $g(t,z_1)$ and $g(t,z_2)$ contribute equally to H_D, where

$$g(t,z_1)\Big|_{t=-(z_1+z_2)/2} = \int_{-\infty}^{t} dt_1(t-t_1)\; n_z(-2t_1-z_1) \;= \frac{1}{4}\int_0^{\infty} \tau d\tau\; n_z(\tau+z_2) \quad . \tag{4.9}$$

Therefore,

$$H_D \;\simeq\; 1+\frac{4Nr_e}{\gamma}\left[\frac{\int rdr\; n_{r0}^3}{\int rdr\, n_{r0}^2}\right]\int\!\!\int dz_1\, dz_2\; n_z(z_1)\; n_z(z_2)\int_0^{\infty}\tau d\tau\; n_z(\tau+z_2)$$

$$= 1+\frac{4Nr_e}{\gamma}\left[\frac{\int rdr\; n_{r0}^3}{\int rdr\, n_{r0}^2}\right]\int_0^{\infty} dz\int_0^{\infty}\tau d\tau\; n_z(z)\; n_z(\tau+z) \quad . \tag{4.10}$$

Now we introduce normalized coordinates $\rho = r/\sigma_0$, and $\varsigma = z/\sigma_z$. Then

$$H_D \;=\; 1+D\left[\frac{\int \rho d\rho\; n_{r0}^3}{\int \rho d\rho\, n_{r0}^2}\right]\int_0^{\infty} d\varsigma\int_0^{\infty}\tau d\tau\; n_z(\varsigma)\; n_z(\tau+\varsigma) \quad . \tag{4.11}$$

For Gaussian and uniform distributions, this leads to

$$H_D \;= 1+D\times\left\{\begin{array}{l}\frac{2}{3}\text{ (radially Gaussian)}\\ \frac{1}{2}\text{ (radially uniform)}\end{array}\right\}\times\left\{\begin{array}{l}\frac{1}{\sqrt{\pi}}\text{ (longitudinally Gaussian)}\\ \frac{1}{\sqrt{3}}\text{ (longitudinally uniform)}\end{array}\right\} . \tag{4.12}$$

This formula agrees very well with the simulation results for $D \lesssim 0.5$. Notice that for $D \ll 1$, the empirical expression for H_D in Eq. (3.4) behaves as $D^{15/4}$, which is by no means close to the linear behavior in Eq. (4.12). This is mainly because of the need to suppress the strong $\ell n(1/A)$ dependence in Eq. (3.4)

in the small D regime. This strong $\ell n(1/A)$ dependence, however, is necessary to fit the medium and large D regimes.

Rigorously speaking, H_D cannot be Taylor expanded around $D = 0$. In deriving Eq. (4.4) we have assumed that the first term r_0 on R.H.S. of Eq. (4.3) is much larger than the second term. This is not the case when t becomes large, no matter how small D is. One obvious example is that at the focal point the two terms would become equal. For $D \ll 1$, however, this focal point lies far beyond the tail of the oncoming bunch, thus the subtlety mentioned above is alleviated. To be more explicit, from linear optics it is easy to see that the focal length in the weak focusing regime is proportional to σ_z/D, thus the density of the oncoming beam around the focal point is proportional to $\exp\{-1/2\, D^2\} \ll 1$. Since H_D comes from multiplication of the local densities of the two bunches, the contribution from the focal point is exponentially small.

5. THE TRANSITION REGIME

The transition regime is characterized by the appearance of the second peak in dH_D/dt with relatively short duration. This phenomena also conforms with the fact that in this regime the first focal point lies inside the bulk of the oncoming beam. Because of the strong focusing, the deformation of the oncoming beam cannot be ignored. As we will show later in this section, the leading order correction in D for the target bunch deformation is equivalent to the second order contribution in D to the focusing force. To set the stage for the second order calculations, however, we shall still start with the first order approach where the equation of motion is given by Eq. (4.1). For small x in a Gaussian distribution we have

$$\frac{d^2x}{dt^2} = -\frac{4Nr_e}{\gamma}\frac{x}{2\sigma_0^2}\frac{\exp\left\{-\frac{(2t+z_1)^2}{2\sigma_z^2}\right\}}{\sqrt{2\pi}\,\sigma_z}$$

$$= -\frac{2D}{\sqrt{2\pi}}\frac{x}{\sigma_z^2}\exp\left\{-\frac{(2t+z_1)^2}{2\sigma_z^2}\right\} \quad . \tag{5.1}$$

It suffices to solve the equation

$$\frac{d^2x}{dt^2} = -\frac{2D}{\sqrt{2\pi}}\frac{x}{\sigma_z^2}\exp\left\{-\frac{2t^2}{\sigma_z^2}\right\} \quad , \tag{5.2}$$

which arises from a coordinate transformation from t to $t + z_1/2$. Let us denote the two solutions to Eq. (5.2) by $u_1(t)$ and $u_2(t)$, with initial conditions at $t = -\infty$

$$u_1 = 1 + O\left(\frac{1}{t}\right) \quad , \quad u_2 = t + O\left(\frac{1}{t}\right) \quad , \tag{5.3}$$

respectively. We are interested in the solutions near the focal point, which for $D \lesssim 5$ occurs at $t_0 \sim \sigma_z/D$. By definition, at the focal point $u_1(t_0) = 0$.

Numerical integration then gives the following approximate solution

$$\dot{u}_1(t_0) \simeq -\frac{3}{4}\,\frac{\sqrt{D}}{\sigma_z} \quad , \quad (0.5 \lesssim D \lesssim 5) \quad , \tag{5.4}$$

while

$$u_2(t_0) \;=\; -\frac{1}{\dot{u}_1(t_0)} \;\simeq\; \frac{4}{3}\,\frac{\sigma_z}{\sqrt{D}} \quad , \quad (0.5 \lesssim D \lesssim 5) \quad . \tag{5.5}$$

The last relation comes from the Wronskian property

$$u_1(t)\dot{u}_2(t) - \dot{u}_1(t)u_2(t) \;=\; 1 \quad . \tag{5.6}$$

The general solution to Eq. (5.2) is therefore

$$x \;=\; x_0\,u_1(t) + x_0'\,u_2(t) \quad . \tag{5.7}$$

Transforming back to the original coordinates, we have the solution to Eq. (5.1)

$$x \;=\; x_0\,u_1\left(t+\frac{z_1}{2}\right) + x_0'\,u_2\left(t+\frac{z_1}{2}\right) \quad . \tag{5.8}$$

Generally, $x_0' \ll 1$, so from Eqs.(5.4), (5.5) and (5.8) we see that a particle at z_1 would be focused to the axis at time $t_0 \sim \sigma_z/D$, or

$$t \;\sim\; \frac{\sigma_z}{D} \;-\; \frac{z_1}{2} \quad . \tag{5.9}$$

The focal point is thus at

$$z_2 \;=\; -2t - z_1 \;\sim\; -\frac{2\sigma_z}{D} \quad . \tag{5.10}$$

This means particles at different longitudinal positions z_1 in one bunch would all be focused to the same point $z_2 \sim 2\sigma_z/D$, but at different times.

This naïve picture, however, contradicts simulation results. Two computer analyses were performed to monitor the detail processes of beam focusing in this regime. Figure 6 shows the time evolution of the average radius $\bar{r}(t,z)$ of a set of selected z–slices with z_1 ranging from $-2\sigma_z$ to $+2\sigma_z$ for $D = 1.0$ and $A = 0.05$. Here, $\bar{r}$ is defined as

$$\bar{r} \equiv \left\{ 2 \int_0^\infty [n_r(r)]^2 \, r dr \right\}^{-1/2} , \tag{5.11}$$

where the radial particle distribution function $n_r(r)$ is normalized such that $\int n_r(r) \, r dr = 1$. The above definition is equivalent to the definition of the standard deviation σ_0 in the limit of a Gaussian distribution, but in general it puts more weight on the radii that have higher particle densities. This is particularly inspired by the observation that during the collision, a bunch tends to develop into a core and a halo, and the conventional definition of the *rms* value would not reflect the crucially important role of the core.

One finds in Fig. 6 that most particles at different z's are focused almost simultaneously, at $t \sim 0.8 \, \sigma_z/c$, which differs with Eqs. (5.9) and (5.10). This fact is also reflected by the relatively short duration of the second peak in dH_D/dt. Indeed, the full-width half-maximum (FWHM) of the second peak turns out to be around $0.4 \, \sigma_z/c$ throughout the range of $0.7 \lesssim D \lesssim 3$. One further computer analysis is shown in Fig. 7 for dH_D/dz as a function of z. This is the cumulative contribution of each z–slice of one beam to the luminosity enhancement. If all the particles are focused at the same z_2, as the strong-weak picture suggests, then dH_D/dz must show a sharp spike. On the contrary, Fig. 7 shows a smooth curve manifesting the longitudinal Gaussian distribution of the beam.

To account for these facts, we proceed by including the deformation of the oncoming beam to the first order in D. To this order, the deformation of a longitudinal slice at z_1 is given by Eq. (4.5), and that for the oncoming beam is obtained by simply replacing z_1 by $z_2 = -2t - z_1$, i.e.,

$$n_{r1}(r, t, z_2 = -2t - z_1) \;=\; n_{r0}(r)\left[1 + \frac{4Nr_e}{\gamma}\left(\frac{1}{n_{r0}}\frac{dn_{r0}}{dr}\int f_0 + n_{r0}\right) g(z_1)\right] . \tag{5.12}$$

It is interesting to observe that t does not appear on the R.H.S. of the above equation. We can thus improve the unperturbed equation of motion by replacing $f_0(r)$ with

$$f_1(r, z_1) \;=\; \frac{1}{r}\int_0^r n_{r1}(r, t, z_2 = -2t - z_1)\; r dr \; . \tag{5.13}$$

Substituting Eq. (5.12) into Eq.(5.13), we find a simple expression

$$f_1(r, z_1) \;=\; f_0(r)\left[1 + \frac{4Nr_e}{\gamma}\, n_{r0}(r)\, g(z_1)\right] . \tag{5.14}$$

Actually, the above inclusion of the deformation of the oncoming beam, with the disruption parameter D intact, can also be interpreted as the inclusion of the modification of D to the next order, namely,

$$D \to D\left[1 + \frac{4Nr_e}{\gamma}\, n_{r0}(r)\, g(z_1)\right] , \tag{5.15}$$

with the distribution $f_0(r)$ unchanged. From this viewpoint, the focusing force for the bunch core near the axis is increased by a factor

$$1 + \frac{4Nr_e}{\gamma}\, n_{r0}(r)\, g(z_1) \;=\; 1 + 4D\,\frac{g(z_1)}{\sigma_z} \quad . \tag{5.16}$$

Once this is seen, the result from the strong-weak picture (or the first order expansion in D) can be readily modified to include the next order in D. Namely, the focal point should occur at

$$t \sim \frac{\sigma_z}{D\,[1+4Dg(z_1)/\sigma_z]} - \frac{z_1}{2} \,. \tag{5.17}$$

From the definition of $g(z_1)$, we find for small z_1

$$4\,\frac{g(z_1)}{\sigma_z} = \frac{1}{\sqrt{2\pi}} - \frac{1}{2}\,\frac{z_1}{\sigma_z} + \ldots \quad . \tag{5.18}$$

This implies that the z_1 dependence in Eq. (5.17) is almost cancelled provided that D is not too large (e.g., of order unity). Thus, the minimum beam size occurs at the time

$$t \sim t_f(D) \equiv \frac{\sigma_z}{D\left(1+D/\sqrt{2\pi}\right)} \,. \tag{5.19}$$

We are now ready to derive the luminosity enhancement factor H_D. The beam size of the slice at z_1 can be derived from Eq. (5.8) as

$$\begin{aligned} \sigma_1^2 &= \langle x_0^2 \rangle \; u_1^2\left(t+\frac{z_1}{2}\right) + \left\langle x'^2_0 \right\rangle \; u_2^2\left(t+\frac{z_1}{2}\right) \\ &= \sigma_0^2 \left[u_1^2\left(t+\frac{z_1}{2}\right) + \left(\frac{1}{\beta^*}\right)^2 u_2^2\left(t+\frac{z_1}{2}\right)\right] \quad . \end{aligned} \tag{5.20}$$

Considering that the primary contribution to H_D comes essentially from the high particle densities near the focii of both bunches, we concentrate on the beam size around $t \simeq t_f(D)$, where $u_1(t_f) = 0$. Thus, Eq. (5.20) becomes

$$\sigma_1^2 \simeq \sigma_0^2 \left\{ \left[\dot{u}_1(t_f)\right]^2 (t-t_f)^2 + \left[\frac{u_2(t_f)}{\beta^*}\right]^2 \right\}$$

$$= \sigma_0^2 \left[\frac{9D}{16} \left(\frac{t - t_f}{\sigma_z} \right)^2 + \frac{16A^2}{9D} \right] , \tag{5.21}$$

where Eqs. (5.4) and (5.5) have been used. The same expression holds for σ_2^2 of the second beam near $t \simeq t_f$. The enhancement factor is therefore

$$\begin{aligned} H_D &= \int dz_1\, dz_2\, \frac{1}{2\pi\, \sigma_z} \exp\left\{ -\frac{z_1^2 + z_2^2}{2\sigma_z^2} \right\} \left[\frac{2\sigma_0^2}{\sigma_1^2 + \sigma_2^2} \right] \\ &= 2 \int ds\, dt\, \frac{1}{2\pi\, \sigma_z} \exp\left\{ -\frac{s^2 + t^2}{\sigma_z^2} \right\} \left[\frac{9D}{16} \left(\frac{t - t_f}{\sigma_z} \right)^2 + \frac{16A^2}{9D} \right]^{-1} \\ &= \frac{1}{\sqrt{\pi}} \int \frac{dt}{\sigma_z} \exp\left\{ -\frac{t^2}{\sigma_z^2} \right\} \left[\frac{9D}{16} \left(\frac{t - t_f}{\sigma_z} \right)^2 + \frac{16A^2}{9D} \right]^{-1} . \end{aligned} \tag{5.22}$$

Since the contribution to H_D essentially comes from around $t \sim t_f$, we can approximately carry out the above integral as

$$H_D \simeq \frac{\sqrt{\pi}}{A} \exp\left\{ \frac{-1}{\left[D \left(1 + D/\sqrt{2\pi} \right) \right]^2} \right\} . \tag{5.23}$$

Unfortunately, this expression does not fit the transition regime in Fig. 4 too well numerically. In particular, it is too sensitive to A, and Eq. (5.22) gives too sharp a peak in dH_D/dt. The disagreement mainly comes from the fact that t_f is not strictly z_1 independent. The residual z_1 dependence in Eq. (5.17) would break the simultaneity of focusing among all the z–slices. As a result, at time t_f when a slice at z_1 reaches its minimum size σ_1, the overlapping oncoming slice at z_2 may not have reached its minimum yet. This slight mismatch between σ_1 and σ_2 would potentially relax the sensitivity of H_D on A as in Eq. (5.23).

To incorporate the residual z_1 dependence in t_f, numerical integration will be needed. Our result here, however, does indeed qualitatively explain the essential

physical process which dominates the transition regime. Namely, the luminosity in the transition regime is contributed primarily from a very narrow window of collision time when the longitudinal slices from head to tail of each bunch are focussed to their minimum size almost simultaneously.

6. PINCH CONFINEMENT OF BUNCH CORE

In the large D regime ($D \gtrsim 5$), the most striking phenomena is the *confinement* of a large fraction of bunch particles near the axis within a small equilibrium radius throughout the course of collision. We call this portion of the bunch the *core,* as opposed to the *halo* particles that come from either being never focused to the axis or being focused but escaped. The occurance of this phenomena, however, is nothing like a phase transition that appears abruptly at a particular value of D. In fact, we already see certain signature from the slices near the bunch tail in Fig. 6, where slices at $z = -1.0,\ -1.5$ and -2.0 tend to stay at a pinched radius. This is why we called the regime for medium D the transition regime.

In this section we devise an analytic description of the large D regime guided by simulation results. Since the luminosity essentially comes from the confined core, we will emphasize the behavior of the core. This is handled, again, by the mean radius $\bar{r}$ of a longitudinal slice introduced in Eq. (5.11). However, for the sake of mathematical simplicity, the transverse distributions of each longitudinal slice is assumed to be Gaussian at any time. The evolution of the beam size is described by the *rms* beam size $\sigma_j(z_j, s)$ of a slice at z_j that comes to s. Since we assume equal beams, we have by mirror symmetry

$$\sigma_1(z, s) = \sigma_2(z, -s) \quad . \tag{6.1}$$

In the linear approximation of the focusing force, the equation of motion of a particle at z_1 in the first beam is given by

$$\frac{d^2x}{ds^2} + K_1\ (z_1, s)\ x = 0 \quad , \tag{6.2}$$

with

$$K_1(z_1,s) = \frac{2Nr_e}{\gamma}\left[\frac{n_z(z_2)}{[\bar{\sigma}_2(z_2,s)]^2}\right]_{z_2=z_1-2s} \quad . \tag{6.3}$$

When D is very large, the actual beam size is rapidly oscillating during the collision. We may smooth out this fluctuation in the focusing force K_1. In this sense we have introduced $\bar{\sigma}_2$ in Eq. (6.3), where the bar indicates a smoothing over some short interval of s. Our task is to solve Eq. (6.2) to obtain $x(z_1,s)$ and from which to deduce the beam size σ_1 so as to be self-consistent with $\bar{\sigma}_2$ in K_1.

In the case where D is very large and the particle in consideration is well inside the oncoming bunch (i.e., $|z_2| \lesssim$ (some factor) $\times\sigma_z$), the WKB approximation is suitable to solve Eq. (6.2). Thus, in this case we have

$$x(z_1,s) \simeq \frac{\sigma_0}{[\sigma_z^2\ K_1(z_1,s)]^{1/4}}\ (C_1\cos\theta_1 + C_2\sin\theta_1) \quad , \tag{6.4}$$

where

$$\theta_1 = \int_{s_0}^{s} \sqrt{K_1(z_1,s)}\ ds \quad . \tag{6.5}$$

Here, we have introduced dimensionless constants C_1 and C_2. In order to express them in terms of the initial condition x_0 and x_0', we need a solution near the head of the oncoming bunch, where WKB fails. This will be discussed later.

Since $\cos\theta_1$ and $\sin\theta_1$ oscillate very rapidly, we may put $\overline{\cos^2\theta_1} = \overline{\sin^2\theta_1} = 1/2$ and $\overline{\cos\theta_1\sin\theta_1} = 0$. Then, we have

$$\overline{x^2(z_1,s)} = \frac{\sigma_0^2}{\sigma_z\sqrt{K_1(z_1,s)}}\ \frac{1}{2}(C_1^2 + C_2^2) \quad . \tag{6.6}$$

To get the smoothed beam size we average Eq. (6.6) over the initial distribution, from which we get

$$\bar{\sigma}_1^2(z_1,s) = \langle \overline{x^2(z_1,s)} \rangle = \frac{C\ \sigma_0^2}{\sigma_z\ \sqrt{K_1(z_1,s)}} \quad , \tag{6.7}$$

with

$$C = \left\langle \frac{1}{2}\ (C_1^2 + C_2^2) \right\rangle \quad , \tag{6.8}$$

where $\langle\ \rangle$ denotes the average over the initial distribution. Then, we get from Eqs. (6.3) and (6.7)

$$\bar{\sigma}_1^2(z_1,s) = \frac{C}{\sqrt{2D}}\ \left[\frac{\sigma_0\ \bar{\sigma}_2(z_2,s)}{\sqrt{\sigma_z n_z(z_2)}}\right]_{z_2=z_1-2s} \quad . \tag{6.9}$$

Similarly, for the second beam

$$\bar{\sigma}_2^2(z_2,s) = \frac{C}{\sqrt{2D}}\ \left[\frac{\sigma_0\ \bar{\sigma}_1(z_1,s)}{\sqrt{\sigma_z n_z(z_1)}}\right]_{z_1=z_2+2s} \quad . \tag{6.10}$$

Now, we can solve Eqs. (6.9) and (6.10) self-consistently with the result

$$\bar{\sigma}_1(z_1,s) = \frac{C\sigma_0}{\sqrt{2D}}\ \left[\sigma_z n_z(z_1)\right]^{-1/6}\ \left[\sigma_z n_z(z_2)\right]^{-1/3}_{z_2=z_1-2s} \quad . \tag{6.11}$$

Inserting into Eq. (6.3) we obtain

$$K_1(z_1,s) = \frac{4D^2}{C^2\sigma_z^2}\ \left[\sigma_z n_z(z_1)\right]^{2/3}\ \left[\sigma_z n_z(z_2)\right]^{4/3}_{z_2=z_1-2s} \quad . \tag{6.12}$$

Here, we have a remarkable formula saying that the beam size is determined only by local variables, namely, the longitudinal density of the beam of interest at z_1

and the longitudinal density of the oncoming beam at the same position. All the history of the particle is packed in one single parameter C. Keep in mind, however, that Eqs. (6.11) and (6.12) do not apply to the head and the tail of the bunches.

Figure 8 shows the time evolution of the beam size for five z–slices at $z_1 =$ 1.0, 0.5, 0, -0.5 and $-1.0\ \sigma_z$, for $D = 100$ and $A = 0.05$. These five curves are then overplotted in Fig. 8(f). One finds that there is no distinctive difference among the five curves except for the shift in time according to their locations in the bunch. The slices abruptly shrink when entering the oncoming beam and soon reach some equilibrium "core" with small and rapid wiggles and a slow variation of the mean radii. The rapid wiggles are related to the oscillations of $\cos\theta_1$ and $\sin\theta_1$, whereas the slow variation agrees well with $[n_z(z_2)]^{-1/3} \propto \exp\left[(z_1 - 2s)^2/6\sigma_z^2\right]$ in Eq. (6.11), which ensures the validity of the WKB approximation.

In order to find H_D we have to express C_1, C_2 and C in terms of the initial conditions. To this end we need a drastic approximation. The fact that the beam size suddenly reduces to a small value suggests that we may ignore the focusing force before the particles are focused to the core. Therefore, we shall assume that the focusing force K_1 is given by Eq. (6.12) when z_2 is well inside the oncoming beam but it is zero near the beginning and the end of the collision. The boundary is determined by the limit where WKB fails. The condition that the WKB is valid is given by

$$\left|\frac{d}{ds}\,\frac{1}{\sqrt{K_1}}\right| \lesssim 1 \quad . \tag{6.14}$$

Since z_1 is a constant for a given particle, we can rewrite Eq. (6.12) as

$$K_1 = \frac{k^2}{\sigma_z^2} \exp\left\{-\frac{8s'^2}{3\sigma_z^2}\right\} \quad , \tag{6.15}$$

with

$$\begin{cases} s' = s - \frac{z_1}{2} \quad , \\ k = \sqrt{\frac{2}{\pi}}\,\frac{D}{C} \exp\left\{-\frac{z_1^2}{6\sigma_z^2}\right\} \end{cases} \quad . \tag{6.16}$$

We shall ignore $\exp(-z_1^2/6\sigma_z^2)$, assuming that our particle is nowhere near the head and the tail of the beam. The solution of Eq. (6.14) for $s' < 0$ is

$$s' \gtrsim s_0' \quad , \tag{6.17}$$

where $s_0'(< 0)$ is a solution to

$$\frac{8(-s_0')}{3\ k\ \sigma_z} \exp\left\{\frac{4s_0'^2}{3\sigma_z^2}\right\} = 1 \quad , \tag{6.18}$$

and is approximately given by

$$\frac{s_0'}{\sigma_z} \simeq -\sqrt{\frac{3}{8}\,\ell n\left(\sqrt{\frac{3}{8\pi}}\,\frac{D}{C}\right)} \quad . \tag{6.19}$$

The above s_0' is thus the boundary that partitions the two zones for zero and finite K_1's. Note that at $s' = s_0'$ K_1 is given by

$$K_1(s_0') = \frac{9}{32\pi}\left(\frac{k}{\sigma_z C}\right)^2\left(\frac{\sigma_z}{s_0'}\right)^2 \simeq \frac{3}{2\pi^2}\left(\frac{D}{\sigma_z C^2}\right)^2\left[\ell n\left(\sqrt{\frac{3}{8\pi}}\,\frac{D}{C}\right)\right]^{-1} \quad . \tag{6.20}$$

The solution with the initial condition x_0 and x_0' at $s' = s_0'$ is then

$$x = x_0 \left[\frac{K_1(s_1')}{K_1(s')}\right]^{1/4} \cos\theta + x_0' \left[\frac{1}{K_1(s_0')\ K_1(s')}\right]^{1/4} \sin\theta \quad , \tag{6.21}$$

where

$$\theta = \int_{s_0'}^{s'} \sqrt{K_1(s')}\ ds' \quad . \tag{6.22}$$

Note that we have ignored the derivative of K_1, which is always valid whenever the WKB approximation is applicable. Rigorously speaking, we should impose the initial condition at $s = 0$, not at $s' = s_0'$. Our treatment is justified because for very small A the deflecting angle x_0' at $s' = s_0'$ is much smaller than σ_0, which is the typical value of x_0.

Comparing Eqs. (6.21) and (6.4) we have

$$\begin{cases} C_1 = \left[\sigma_z^2\ K_1(s_1')\right]^{1/4} \frac{x_0}{\sigma_0} = \left[\frac{2}{3}\left(\frac{\pi C^2}{D}\right)^2\ \ell n\left(\sqrt{\frac{3}{8\pi}}\ \frac{D}{C}\right)\right]^{-1/4} \frac{x_0}{\sigma_0} & (6.23) \\ C_2 = \left[\sigma_z K_1(s_1')\right]^{-1/4} \frac{\sigma_z x_0'}{\sigma_0} \quad . & (6.24) \end{cases}$$

Averaging over the initial distribution gives

$$\langle C_1^2 \rangle = \frac{D}{\pi C^2} \left[\frac{2}{3}\ \ell n\left(\sqrt{\frac{3}{8\pi}}\ \frac{D}{C}\right)\right]^{-1/2} \quad , \tag{6.25}$$

and

$$\langle C_1^2 \rangle\ \langle C_2^2 \rangle = \frac{\langle x_0^2 \rangle}{\sigma_0^2}\ \frac{\sigma_z^2\ \langle x_0'^2 \rangle}{\sigma_0^2} = A^2 \quad . \tag{6.26}$$

The latter merely insures the conservation of the linear emittance. Since we assume $A \ll 1$ and $D \gg 1$, we have $\langle C_1^2 \rangle \gg \langle C_2^2 \rangle$. Therefore,

$$C^2 = \frac{1}{2} \langle C_1^2 + C_2^2 \rangle \simeq \frac{1}{2} \langle C_1^2 \rangle \quad , \tag{6.27}$$

which, together with Eq. (6.25), determines C self-consistently. We now get

$$C = \left(\frac{D}{2\pi} \right)^{1/3} \left[\frac{2}{3} \ell n \left(\sqrt{\frac{3}{8\pi}} \, \frac{D}{C} \right) \right]^{-1/6} \quad . \tag{6.28}$$

While C still appears on the RHS of the expression, it varies only logarithmically. We may substitute C on RHS with some constant times $D^{1/3}$. As a good approximation we get

$$C = \left(\frac{3D}{4\pi} \right)^{1/3} \left[\ell n \left(\frac{D}{2} \right) \right]^{-1/6} \quad , \tag{6.29}$$

which agrees with the exact solution of Eq. (6.28) within 1% for $D \gtrsim 10$. Thus, the smoothed beam size in Eq. (6.11) is now written as

$$\bar{\sigma}_1(z_1, s) = \sigma_0 \left[\frac{9}{32\sqrt{2\pi}} \, \frac{1}{D \ell n(D/2)} \right]^{1/6} \exp \left\{ \frac{z_1^2 + 2z_2^2}{12\sigma_z^2} \right\}_{z_2 = z_1 - 2s} \quad , \tag{6.30}$$

and the focusing function is

$$K_1(z_1, s) = \left[\frac{128}{9\pi} \, D^4 \, \ell n \left(\frac{D}{2} \right) \right]^{1/3} \exp \left\{ \frac{z_1^2 + 2z_2^2}{3\sigma_z^2} \right\}_{z_2 = z_1 - 2s} \quad . \tag{6.31}$$

These formulas apply for

$$|z_2| \lesssim 2|s_0'| \simeq \sqrt{\frac{3}{2} \ell n \left(\frac{D}{2} \right)} \, \sigma_z \quad . \tag{6.32}$$

Let us now calculate the enhancement factor H_D. Analogous to Eq. (5.23) we have

$$H_D = \int dz_1 dz_2 \, \frac{\sigma_0^2}{\sigma_1^2(z_1,s)+\sigma_2^2(z_2,s)} \, \frac{1}{\pi\sigma_z^2} \, \exp\left\{\frac{z_1^2+z_2^2}{2\sigma_z^2}\right\}_{z_2=z_1-2s} . \quad (6.33)$$

Note that $2\,dsdt = dz_1 dz_2$. If we replace σ_j in this expression with the smoothed radius $\bar{\sigma}_j$ in Eq. (6.29), we get

$$\overline{H}_D = 1.374 \left[D\,\ell n\left(\frac{D}{2}\right)\right]^{1/3} \quad (6.34)$$

via numerical integration. As in the case of the transition regime where the slight mismatch between σ_1 and σ_2 should not be overlooked, in the confinement regime the rapid wiggling of the beam size also plays some role and, therefore, one needs to use σ_j instead of $\bar{\sigma}_j$. Averaging the square of Eq. (6.4) over the initial distribution and using Eqs. (6.25) and (6.30), we get

$$\begin{aligned}\sigma_1^2(z_1,s) &\equiv \langle x_1^2(z_1,s)\rangle \\ &= \sqrt{2\pi}\,\frac{\sigma_0^2}{D}\left(C^2\cos^2\theta_1 + \frac{A^2}{4}\sin^2\theta_1\right) \exp\left\{\frac{z_1^2+2z_2^2}{6\sigma_z^2}\right\}_{z_2=z_1-2s} .\end{aligned} \quad (6.35)$$

At $\theta_1 = \pi/2$, we have the minimum beam size $\sigma_1 \simeq [(2\pi)^{1/4}\, A/2\sqrt{D}]\sigma_0$, as stated in Eq. (3.3). Notice that if we ignore A^2 and replace $\cos^2\theta_1$ by $1/2$, we recover the smoothed beam size in Eq. (6.30). Nevertheless, the finiteness of A can still contribute to the luminosity near the zeros of $\cos\theta_1$. Substituting Eq. (6.35) into Eq. (6.33), the new H_D now reads

$$H_D = \frac{D}{\pi\sqrt{2\pi}} \int \frac{dz_1 dz_2}{\sigma_z^2} \exp\left\{-\frac{3(z_1^2+z_2^2)}{4\sigma_z^2}\right\}$$
$$\times \left[\exp\left\{\frac{-z_1^2+z_2^2}{12\sigma_z^2}\right\}\left(C^2\cos^2\theta_1 + \frac{A^2}{4}\sin^2\theta_1\right)\right.$$
$$\left. + \exp\left\{\frac{z_1^2-z_2^2}{12\sigma_z^2}\right\}\left(C^2\cos^2\theta_2 + \frac{A^2}{4}\sin^2\theta_2\right)\right]^{-1}_{z_2=z_1-2s} . \tag{6.36}$$

Since θ_1 and θ_2 are strong functions of z_1 and z_2, and $C^2 \gg A^2/4$, we can approximately integrate the above expression to obtain

$$H_D = -\frac{2D}{\pi^2\sqrt{2\pi}\,C^2} \int \frac{dz_1 dz_2}{\sigma_z^2} \exp\left\{-\frac{3(z_1^2+z_2^2)}{4\sigma_z^2}\right\} \ell n\left[\frac{A}{\sqrt{2}\,C}\cosh\left(\frac{z_1^2-z_2^2}{12\sigma_z^2}\right)\right] \tag{6.37}$$

for $A \ll C$. By numerical integration and by invoking Eq. (6.29), we finally obtain

$$H_D = \lambda_1 \left[D\,\ell n\left(\frac{D}{2}\right)\right]^{1/3}\left\{\frac{1}{6}\,\ell n\left[\frac{D^2}{\lambda_2\,\ell n\,(D/2)}\right] - \ell n A\right\} , \tag{6.38}$$

where $\lambda_1 = 0.880$ and $\lambda_2 = 2.28$. The agreement with the simulation is not very excellent but the $\ell n A$ dependence is correctly expressed. We can also obtain dH_D/dt discussed in Section 3 by replacing $dz_1 dz_2$ in Eq. (6.37) with 2 $dsdt$ and by integrating over s. Since only small $|z_1|$ and $|z_2|$ contribute in the integral, we may ignore the variation of cosh in Eq. (6.37) as a rough approximation. In so doing, we obtain

$$\frac{dH_D}{dt} \simeq \frac{\sqrt{3}}{\sqrt{2\pi}\sigma_z} H_D \exp\left\{-\frac{3t^2}{2\sigma_z^2}\right\} . \tag{6.39}$$

Comparing this expression with the unperturbed dH_0/dt of Eq. (3.8), one finds that dH_D/dt for large D is indeed Gaussian with a slightly larger coefficient

for t^2 in the exponent. This fact agrees with the simulation results quite well. (Compare the figure for $D = 100$ versus that for $D = 0.2$ in Fig. 5.) Notice that the functional behavior $\exp(-3t^2/2\sigma_z^2)$ comes solely from the WKB part. On the other hand, the overall factor in Eq. (6.39), which comes from the truncation of K_1 at the head of the bunch, like the case for H_D, does not numerically reproduce the simulation results.

7. DISCUSSION

In this paper we have presented the simulation results of the enhancement factors for the disruption angles and the luminosity. We have shown that the inherent beam divergence, manifested by the newly introduced parameter A, plays a critical role in addition to the well-known disruption parameter D. In particular, while it is the small D regime that is sensitive to A in the case of H_θ, on the contrary, it is the large D regime that is sensitve to A in the case of H_D.

All these observations are then theoretically described with guidance from a further computer analysis of the beam-beam interaction process. Our theory explains the essential features found from computer simulations, although it fails to reproduce H_D numerically in the transition and the confinement regimes.

To summarize, in the weak focusing regime $\left(0 < D \lesssim 0.5\right)$ the enhancement of luminosity comes from the overall deformation of the beam, and is rather insensitive to A. In the transition regime $\left(0.5 \lesssim D \lesssim 5\right)$, the dominant contribution to H_D comes from the high particle densities around the focii that lie within the oncoming beam. The focused particles tend to be severely disrupted afterwards, although when approaching larger D in this regime one starts to observe partial confinement for slices near the tail of the bunch. One novel feature in this regime is that the focusing process tends to occur at the same *time* for different longitudinal slices, but not at the same *position* in the oncoming bunch. This fact is reflected by a sharp spike in the dH_D/dt plots for smaller D, and a sharp rise followed by a wide skirt (from partial confinement) for larger D. These are explained by including the mutual deformations of both beams up to the second-order expansion in D.

The most striking phenomena occurs in the pinch confinement regime $(D \gtrsim 5)$ where a large fraction of the bunch particles are abruptly pinched to a much smaller cross section and tend to be confined within the equilibrium radius throughout the collision process. This fact is well described by the WKB approximation during the confinement, and by the drastic approximation made in the focusing force near the boundary. One major claim from our theory is that during the confinement phase the motion of the particles is adiabatic so that the variation of the oscillation amplitude is determined solely by the local density of both beams and is independent of their history.

In our linearized model for the focusing force in the confinement regime, the bunch core preserves the initial emittance, which in turn provides a thermal energy that is balanced with the potential energy, and gives rise to an equilibrium radius for the core. It can be seen from Eq. (6.35) that, while the upper bound of the oscillation amplitude is governed by C which is independent of A, the lower bound is governed by A. This is confirmed by a plot similar to Fig. 8, but with $D = 100$ and $A = 0.2$. Figure 9 shows that the amplitude of the wiggles is indeed smaller for larger A. In fact, our theory implies that as $A \to 0$ the lower bound vanishes and in turn H_D diverges logarithmically, which agrees with our simulation results.

A closer look at Figs. 8 and 9 indicates that the difference in oscillation amplitudes is not as pronounced as Eq. (6.38) predicts. In addition, there is an obvious smearing of the oscillation during the course of confinement, which is not accounted for by the equation. This suggests that nonlinear terms for the confining potential may be necessary for a better theoretical picture.

Having been demonstrated by the drastically different scenario of our results from previous works, one would naturally ask if our results are prone to various plasma instabilities. One such instability is the *filamentation* instability where local density fluctuations tend to act as tiny focusing lenses that attract the nearby oncoming particles, which in turn further enhance the fluctuations until the beam is eventually torn into clusters. From our simulations, we found no sign of such a filamentation up to $D = 100$. Concerned that our use of axial symmetry to calculate the Poisson equation may have suppressed the effect, we also diagnosed the instability using the band matrix method, which is fully three-dimensional. Due to the constraint on the computing time, however, we had to choose a much larger bin size ($\sim 0.2\ \sigma_0$) at $D = 50$ and 100. Although the results still show no sign of filamentations, it is rather inconclusive because of the coarseness of the bins.

One possibility is that there is a threshold cross section of a beam below which it cannot be further filamented. This threshold beam size has to do with both the energy and the temperature of the beam. For the confined bunch core, we suggested earlier that an equilibrium is rapidly reached between the thermal energy and the potential energy. This might also mean that the equilibrium radius of the core is at or below the filamentation threshold, and no tearing of the core could be possible. As for the halo, notice that it comes from either the particles that are never well focused to the core because of the nonlinear nature of the force associated with Gaussian distributions, or the particles that are *evaporated* from the core for the same reason. In either case, the emittance of the halo must be much larger than the initial value, whence filamentations are also avoided in the halo.

Another possible instability is the *kink* instability where the initial offset of the two beams would be amplified during collision. This instability does exist when D is very large, but should be regarded as a separate issue from what has been studied in this paper. Here our only concern is how beam-beam disruption behaves when the two beams are perfectly aligned.

Finally, there is a digression from the theory we developed for pinch confinement. Recall that H_D is crucially dependent on the parameter C, while C itself is very sensitive to the boundary condition related to the initial stage of the collision. This suggests that perhaps a careful design of the longitudinal particle distribution, especially near the bunch head, would help to achieve the optimum luminosity enhancement.

Acknowledgements

We deeply appreciate many helpful discussions on the subject and comments on the text of the paper from Drs. W. Fawley of LLNL, R. Hollebeek of University of Pennsylvania, and R. B. Palmer, J. Rees, B. Richter, R. D. Ruth and P. B. Wilson of SLAC.

REFERENCES

1. SLC Design Handbook, SLAC (1984); SLAC–Report–229 (1980).
2. R. Hollebeek, Nucl. Instrum. and Meth. **184**, 333 (1981).
3. W. M. Fawley and E. P. Lee, *New Developments in Particle Acceleration Techniques,* S. Turner, ed., CERN87–11 and ECFA87/110, 1987.
4. This discussion on the reduction factor η_A is due to the suggestion of R. D. Ruth.
5. K. Yokoya, KEK Report 85–9 (1985).
6. R. Hollebeek and A. Minten, SLAC Internal Report CN–301 (1985), unpublished; K. Yokoya, SLAC Internal Report AAS–27 (1987), unpublished.
7. P. Chen, SLAC–PUB–4379 (1987), to appear in *Frontiers of Particle Beams,* M. Month, ed., Springer–Verlag, 1988.

FIGURE CAPTIONS

Fig. 1. Schematic diagram that defines the various coordinates of the two colliding bunches. For a test particle in bunch 1 at $z_1 = z$, the relative coordinate with respect to bunch 2 is $z_2 = -2t - z$.

Fig. 2. Maximum disruption angle enhancement factor as a function of D, computed with four different values of A.

Fig. 3. Root–mean–square disruption angle enhancement factor as a function of D. Notice the similar behavior of Figs. 2 and 3, aside from the difference on the numerical values.

Fig. 4. Luminosity enhancement factor as a function of D, computed with five different values of A. The A values are so chosen that they are equally separated on the logrithmic scale.

Fig. 5. Computer analysis on the time evolution of the luminosity enhancement factor H_D, at various different values of D with $A = 0.05$. For very small and very large D's, dH_D/dt varies as a Gaussian function (although for the large D regime there are small wiggles superimposed), while for medium values of D there is an obvious spike.

Fig. 6. Time evolution of the average radius $\bar{r}$ (in units of σ_0) of a set of selected z–slices with z_1 ranging from $-2\ \sigma_z$ to $+2\ \sigma_z$ for $D = 1.0$ and $A = 0.05$. Notice that in this regime of D different slices are focused to their minimum radius at about the same time, in this case, at $t \sim 0.8\ \sigma_z/c$.

Fig. 7. Cumulative contribution of the luminosity enhancement factor dH_D/dz as a function of z. The Gaussian–like distribution indicates the simaltaneity of the focusing process for different z–slices.

Fig. 8. Time evolution of the beam size for five selected z–slices at $z_1 = 1.0,\ 0.5,\ 0,$ -0.5 and $-1.0\ \sigma_z$, for $D = 100$ and $A = 0.05$, shown in the figure from 8(a) to 8(e), respectively. The five figures are then overplotted in 8(f). A *confined* bunch core can be obviously seen.

Fig. 9. A similar plot to Fig. 8, except that $A = 0.2$ in this figure. The behavior of the bunch in this case is almost the same as the one in Fig. 8, other than that the amplitude for the fast oscillations is smaller for larger A.

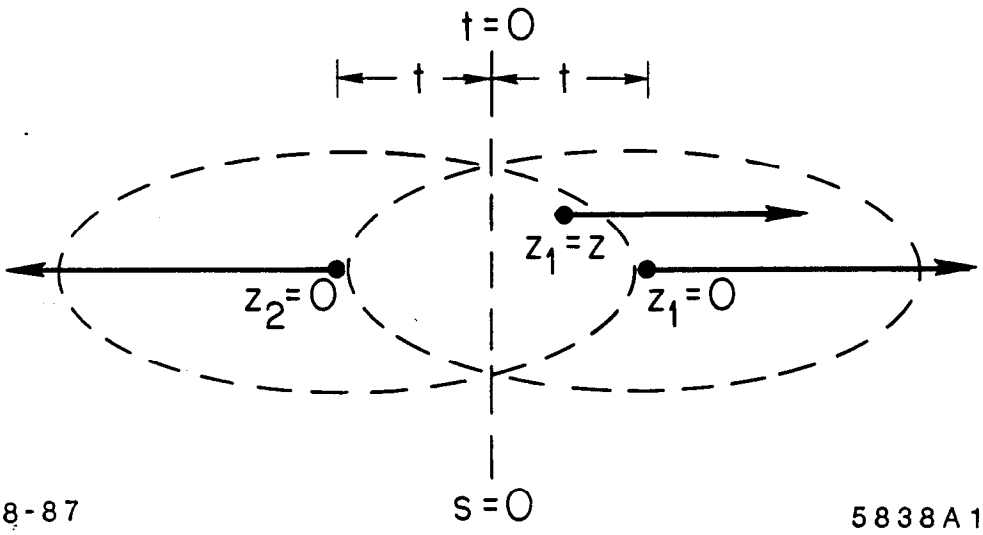

Fig. 1

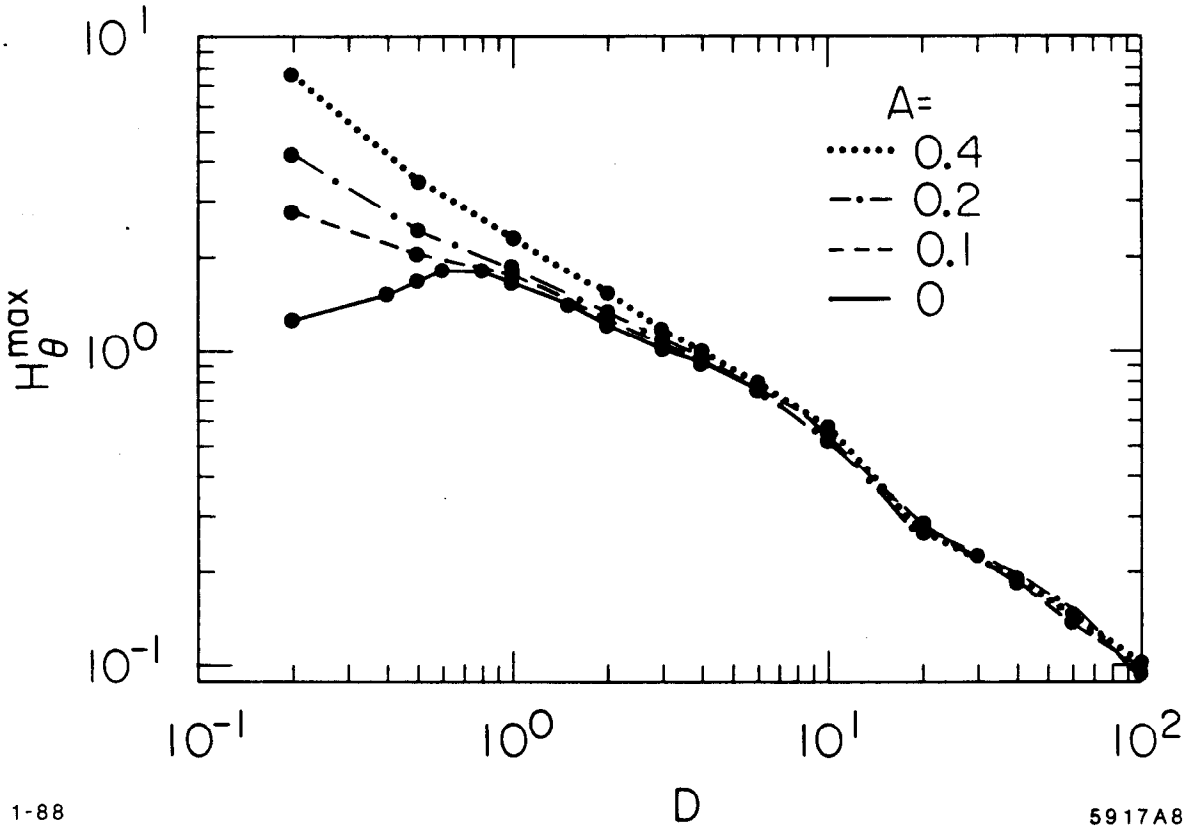

Fig. 2

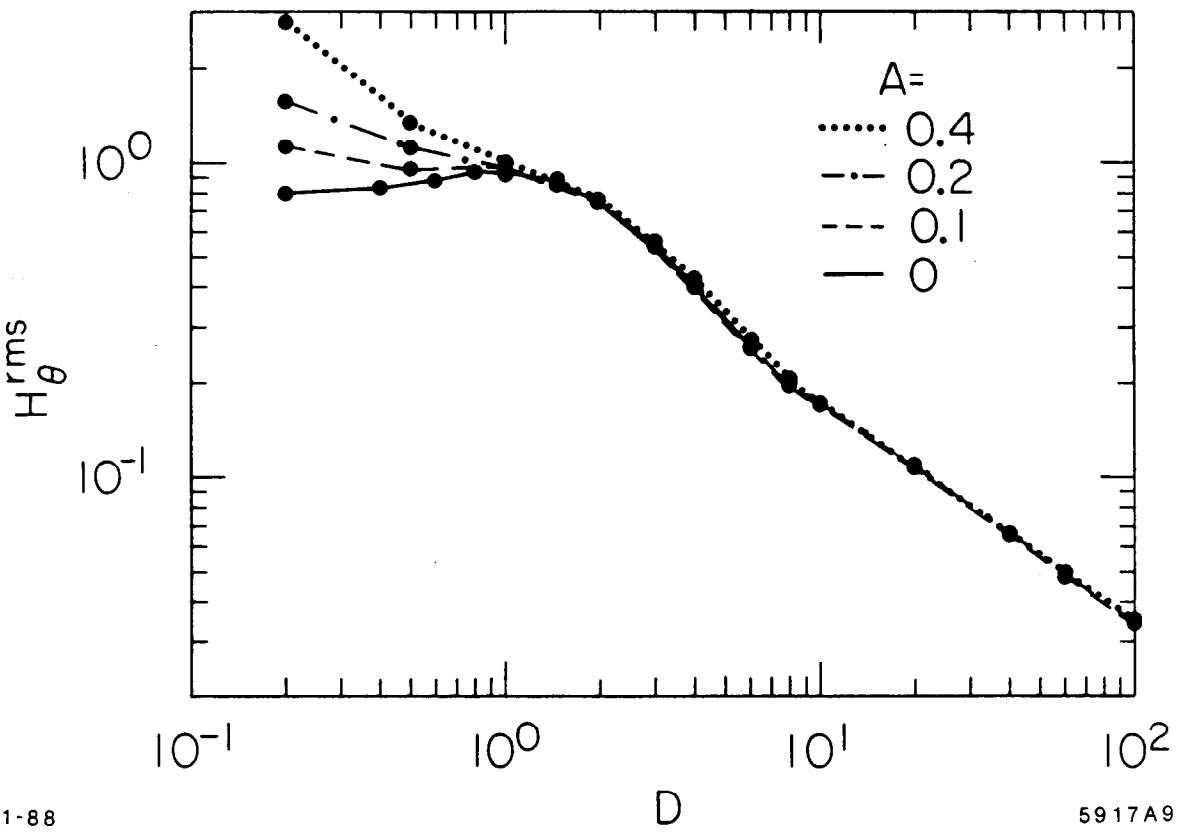

Fig. 3

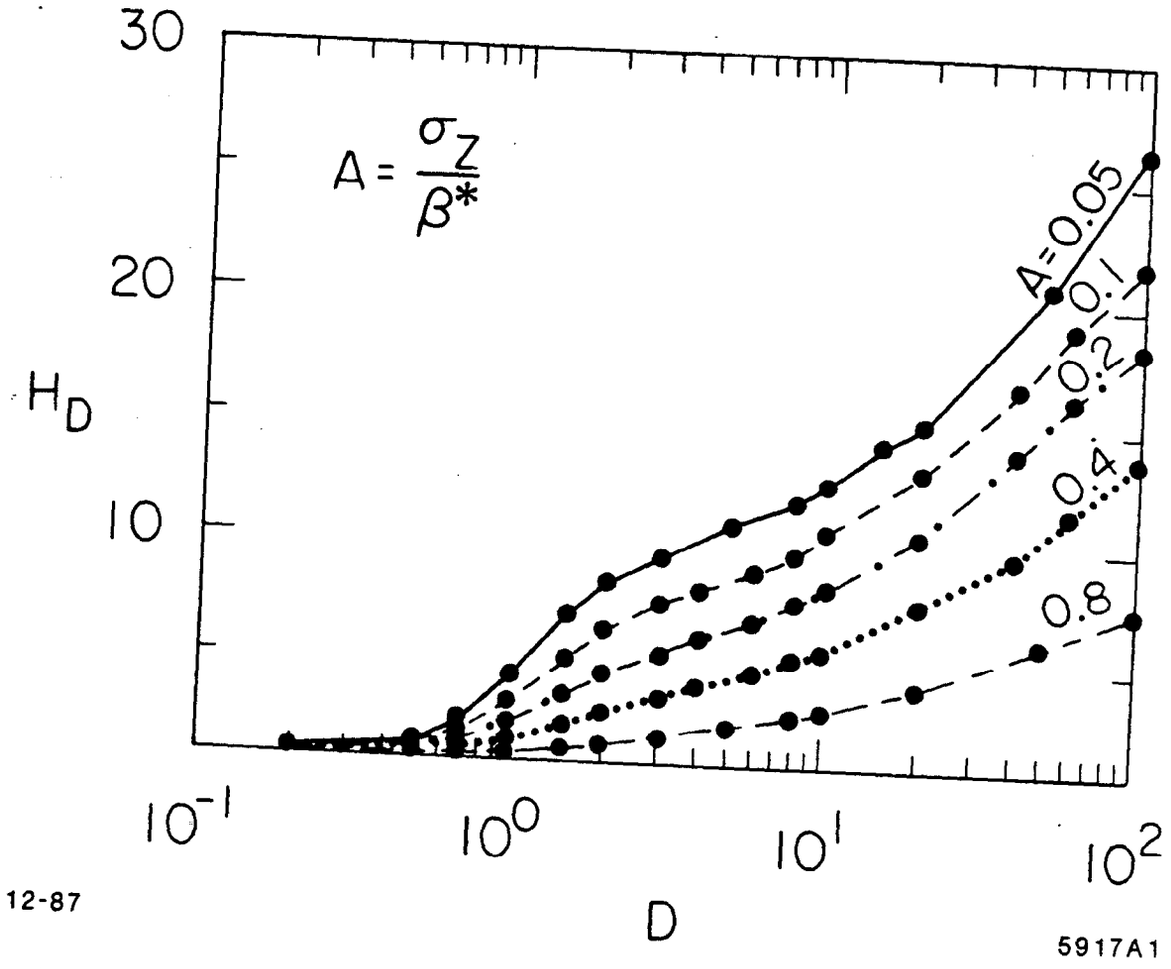
30
20
10
H_D
$A = \frac{\sigma_z}{\beta^*}$
A=0.05
0.1
0.2
0.4
0.8
10^{-1}
10^0
10^1
10^2
D
12-87
5917A1

Fig. 4

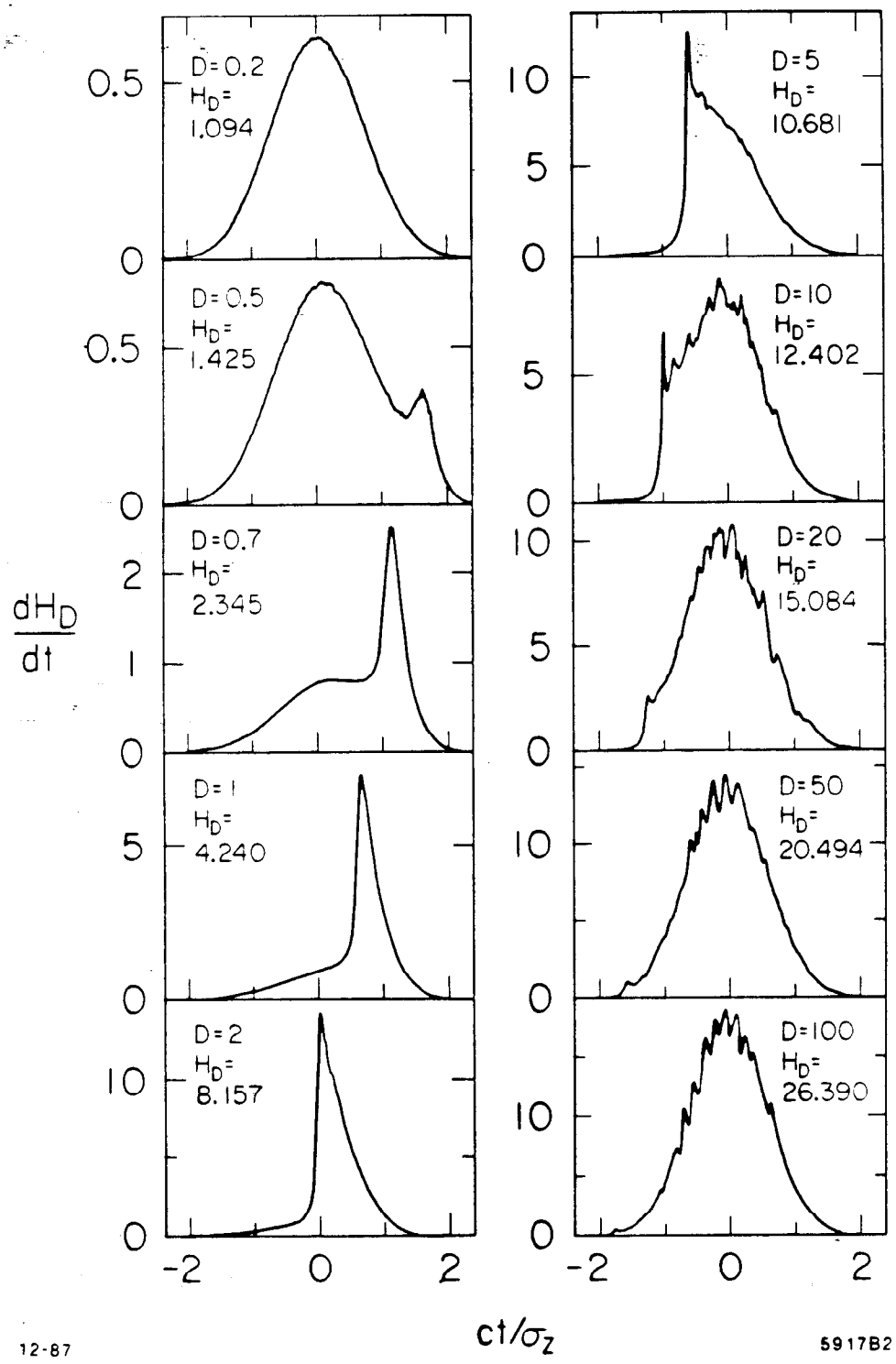
D=0.2
H_D=
1.094
D=0.5
H_D=
1.425
D=0.7
H_D=
2.345
D=1
H_D=
4.240
D=2
H_D=
8.157
D=5
H_D=
10.681
D=10
H_D=
12.402
D=20
H_D=
15.084
D=50
H_D=
20.494
D=100
H_D=
26.390
$\frac{dH_D}{dt}$
ct/σ_z
12-87
5917B2

Fig. 5

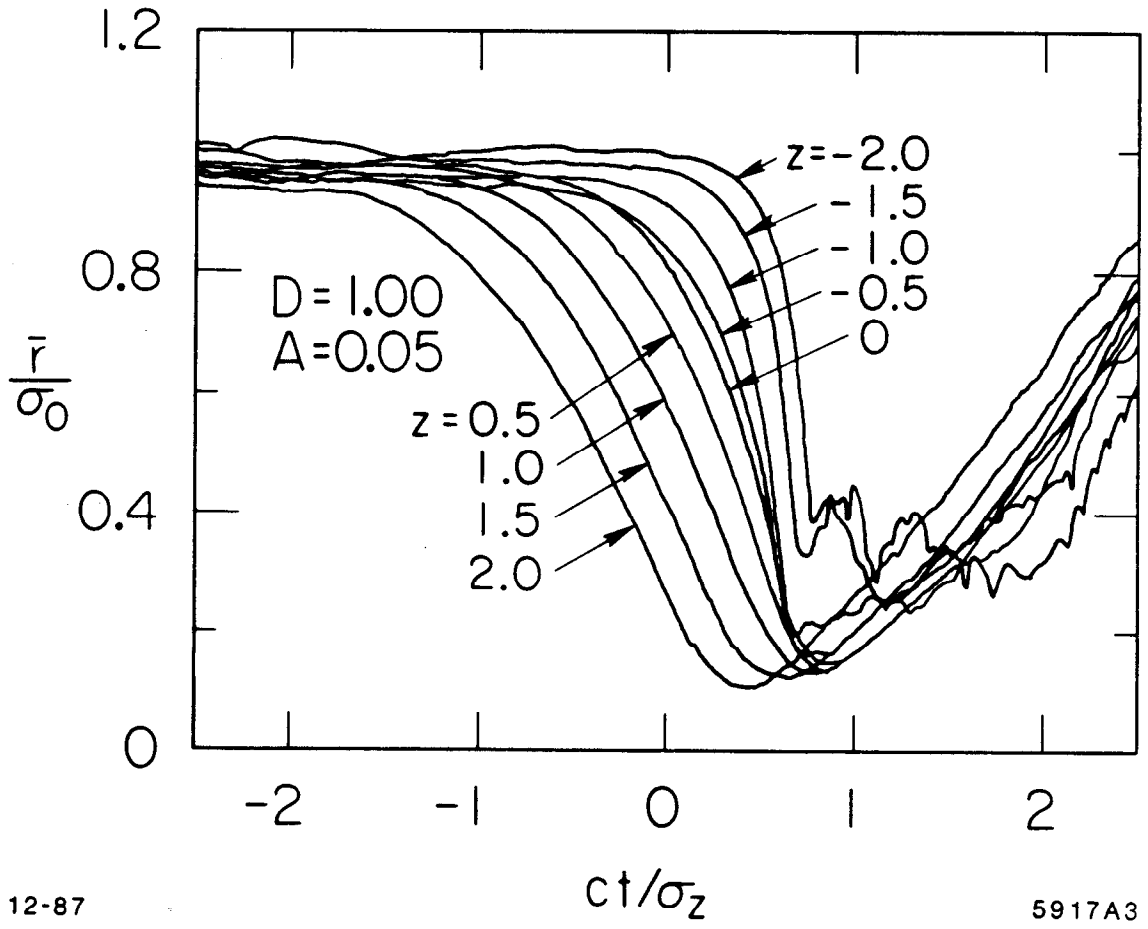
1.2
0.8
0.4
0
$\frac{\bar{r}}{\sigma_0}$
D = 1.00
A = 0.05
z = -2.0
-1.5
-1.0
-0.5
0
z = 0.5
1.0
1.5
2.0
-2
-1
0
1
2
ct/σ_z
12-87
5917A3

Fig. 6

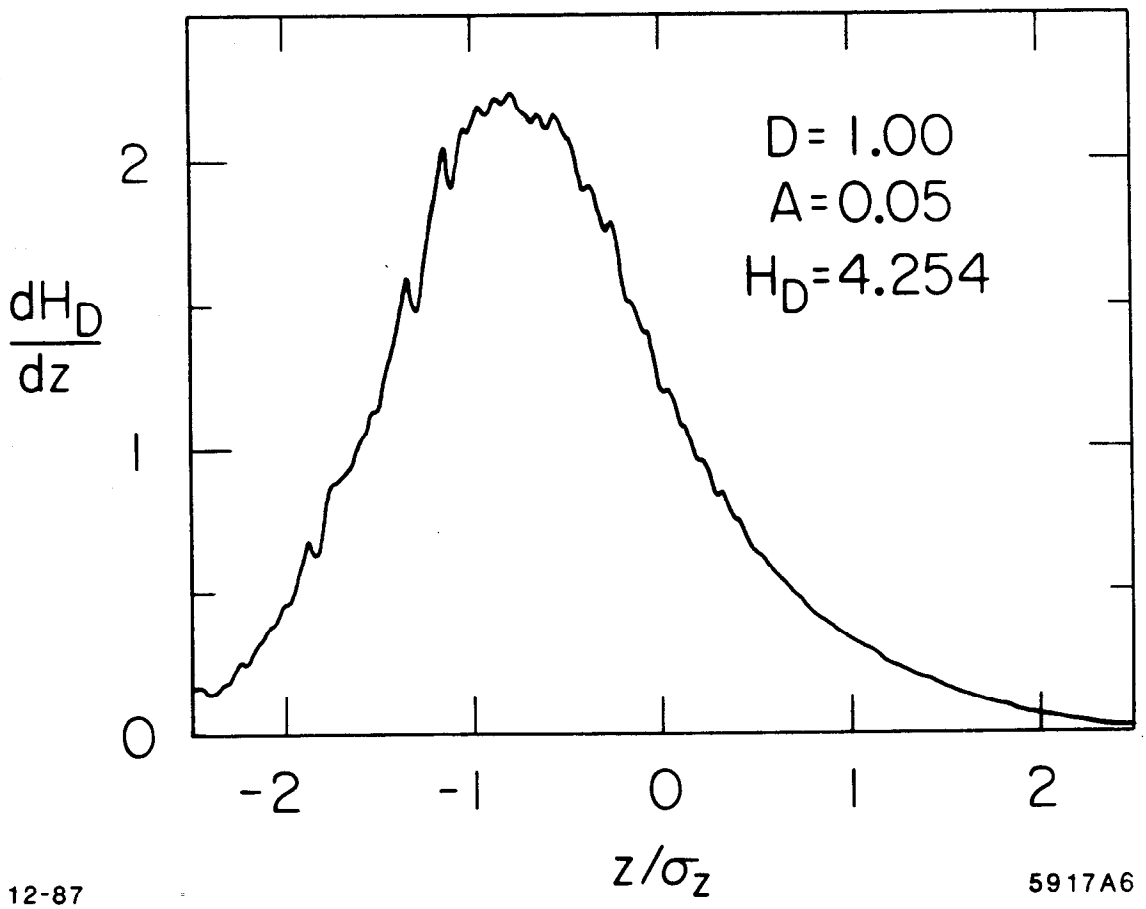

Fig. 7

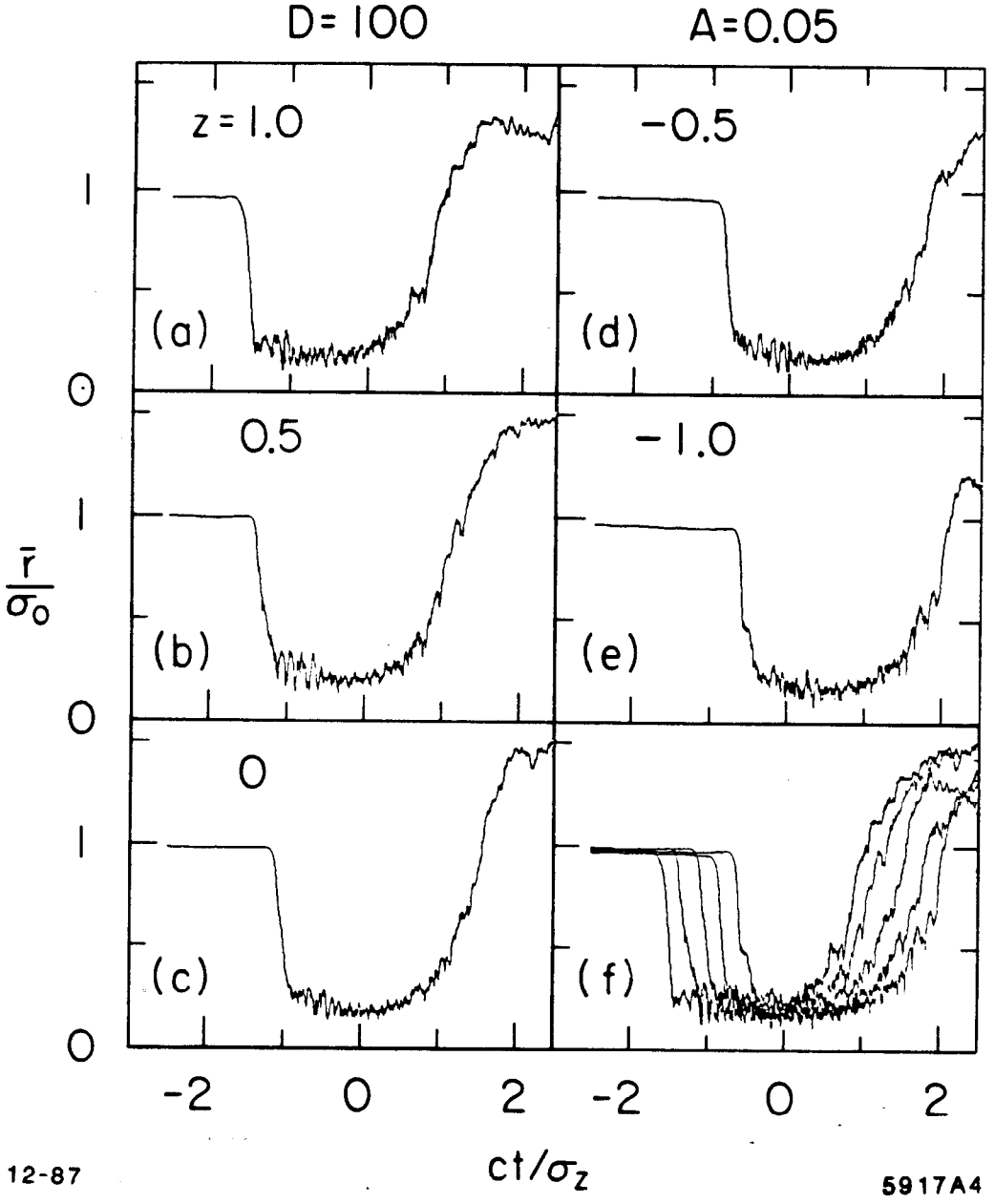
D= 100
A=0.05
z = 1.0
-0.5
0.5
-1.0
0
(a)
(b)
(c)
(d)
(e)
(f)
1
0
1
0
1
0
$\frac{\bar{r}}{\sigma_0}$
-2
0
2
-2
0
2
ct/σ_z
12-87
5917A4

Fig. 8

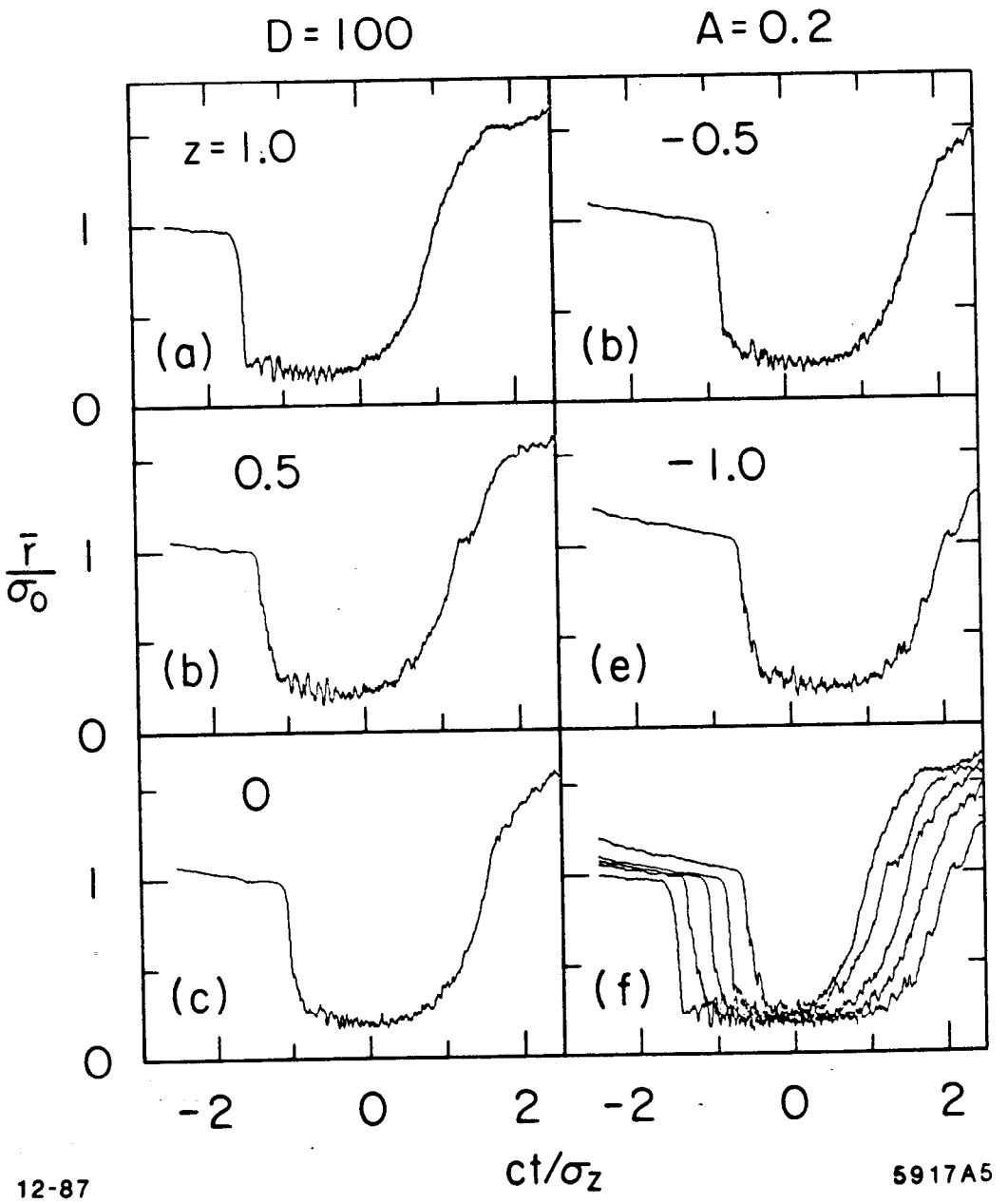
D = 100
A = 0.2
z = 1.0
-0.5
0.5
-1.0
0
(a)
(b)
(b)
(e)
(c)
(f)
1
0
1
0
1
0
$\frac{\bar{r}}{\sigma_0}$
-2
0
2
-2
0
2
ct/σ_z
12-87
5917A5

Fig. 9